

# A Multi-Criteria Design Method of Line-Start PMSM with Enhanced Start-Up Capability for Gantry Crane Lifting Systems

Ioannis D. Chasiotis, *S. Member, IEEE*, Yannis L. Karnavas, *Senior Member, IEEE*,  
Stylianos I. Dimadis, *S. Member, IEEE*

**Abstract** – Line-start permanent magnet synchronous motors (LSPMSMs) are considered as attractive alternatives of induction motors due to their higher efficiency and power factor. Their use is restricted by the fact that their starting performance and synchronization capability are characterized as relatively poor and this does not coincide with the requirements of many industrial applications. In this context, a multi-criteria design approach is proposed aiming to enhance the aforementioned features. For this purpose, a simple algorithm-based design procedure has been developed in order to estimate the rotor bars and magnets geometrical parameters. The derived topologies are evaluated in terms of several performance indices. The obtained results confirm both the effectiveness of the proposed methodology and the feasibility of using LSPMSMs in heavy-duty applications, such as the gantry crane lifting system.

**Index Terms**—line-start permanent magnet synchronous motor, starting performance, synchronization capability, transient finite element analysis, gantry crane.

## I. INTRODUCTION

THE line-start permanent magnet synchronous motors (LSPMSMs) are rapidly replacing the conventional induction motors in several industrial applications, as they present clear advantages over them in terms of efficiency, power factor and power density [1]. The high initial cost for their installation can easily be offset due to the significant savings in energy consumption during their operation. However, their starting and synchronization capability in many cases can be considered as poor [2]. This confirms the fact that they are used in applications, such as fans, pumps, compressor drives, conveyor belts, etc., where high dynamic performance is not required and small torque is provided during the start-up phase [3].

Additionally, the design procedure of the LSPMSMs is characterized by increased complexity as many performance features are conflicting to each other. For instance, a large value for the magnetizing inductance benefits the start-up performance, whereas the synchronization capability is enhanced when a small value for this quantity is used [4]. Furthermore, a large volume for the magnets improves the steady-state performance and guarantees the achievement of high efficiency and power factor. On the other hand, the above contributes to a high braking torque during the asynchronous operation, which reduces the motor's starting capability under load [5]. As a result, dips are showing up in

the average torque and the motor may be tangled in stable region of its torque-speed curve in sub-synchronous speed and oscillated due to the synchronous pulsating torque. Consequently, many compromises have to be made during the design process of the specific motor type [6].

The so far research works have proposed: a) the proper design of the rotor's bars shape [7], b) the use of an asymmetrical cage [8], c) the construction of a canned and slotted rotor [9], d) the development and comparison of new topologies for the permanent magnets [10], [11], e) the analysis of the effect of braking torque, magnetization inductance and demagnetization on the overall performance [12], [13], f) the selection of the proper winding arrangement and the application of a pole changing method [14], g) the study of the hunting phenomenon [15], h) the incorporation of artificial intelligence techniques on the design procedure [16], etc. Despite the fact that some useful design guidelines are provided in [17], the estimation of the optimal parameters still remains a challenge due to the absence of accurate magnetic circuit models for the case of LSPMSMs according to [3]. Moreover, the finite element analysis (FEA) is very time-consuming when the whole search space of all the involved variables is globally considered this way (both in the transient and steady-state phase). Thus, an algorithm-based design optimization may be very useful and could ease the design procedure.

In this paper, a multi-criteria design approach for the calculation of the rotor topology characteristics of a candidate LSPMSM is proposed. The motor is going to be used in a gantry crane application, where high starting-torque is required. For this reason, the investigated configuration has embedded and radially magnetized magnets, as this structure benefits the aforementioned feature [18]. At a first step, the requirements of the specific application are described and a methodology for the calculation of the motor's nominal parameters is given. Next, the stator geometrical characteristics are determined by following the classical design procedure of the induction motors.

Then, a simple algorithm is proposed and applied for the estimation of the permanent magnets dimensions and position. This algorithmic design procedure gives emphasis on the enhancement of motor's starting performance and synchronization capability and needs a small number of iterations until convergence to an optimal machine design solution. At last, aiming to conclude to the final topology, several performance characteristics are examined whereas the overall topology parameters are analytically given. A brief discussion is also made followed by the relevant conclusions.

---

I. D. Chasiotis, Y. L. Karnavas and S. I. Dimadis are with the Electrical Machines Laboratory, Department of Electrical & Computer Engineering, Democritus University of Thrace, Xanthi, Hellas (Greece), GR-671 00, e-mail: ichasiot@ee.duth.gr, karnavas@ee.duth.gr, styldimal@ee.duth.gr.

## II. GANTRY CRANE LIFTING SYSTEM DESCRIPTION

A gantry crane is a type of overhead bridge crane with a single or double girder configuration supported by free standing legs, i.e. legs that either move on wheels or run on a rail system or a track embedded in the ground. Unlike, a typical bridge crane, this system (depicted in Fig. 1) is not tied into a building's support structures and there is no need of permanent run away beams. It presents robust construction and allows the lifting of heavy loads even with the presence of strong winds. The gantry cranes are used in shipyards, rail and container yards, in automotive and fabrication industry and many other either indoors or outdoors heavy-duty industrial applications. The incorporation of electric motors in the hoist mechanism has become very popular, as it provides the following advantages over mechanical counterparts: a) precise control during the transportation of the loads, b) the immediate stop of the motor when the electric power delivery is cut off, c) salient operation, d) increased durability and efficiency for the overall system and e) higher lifting capacity. The motor has to be able to deliver high starting torque and accelerate the loads as smooth as possible. At the same time, it must withstand the frequent brakings, high temperature, operation at dusty environment and possible mishandling by the gantry crane operator.

## III. MOTOR NOMINAL PARAMETERS CALCULATION

The determination of the nominal parameters (i.e. output power and torque) of the investigated LSPMSM comes in accordance with the maximum load mass ( $M_{load}$ ) that the hoist system can carry and the desired speed ( $v$ ) during its moving. In our case, the gantry crane will have a lifting capability of 5,000 kg with a speed of 6 m/min for possible installation in a small indoors industrial facility with height of 6 meters. A repetitive procedure has been followed aiming to calculate the above features. The proposed process is organized as follows:

**Step 1:** “Selection of the number of wire rope's parallel branches”. For indoors applications the use of a wire rope instead of a chain is recommended, as it provides higher lifting capability and permits the development of higher speeds. The selection of this quantity is made along with the data presented in Table I for the case of a double drum wire rope, where the number of parallel branches ( $N$ ) and the efficiency of the overall hoist system are given as a function of the load mass. Thus, in this step, a wire rope with four branches has been selected.

**Step 2:** “Estimation of the hoist system's total mass”. In order to calculate the load that each parallel branch will carry, we have to analyze the individual components of the winch. It consists of the wire rope, the hook and two pulleys. Taking into account the characteristics of commercially available hooks of class "T" with similar specifications the hook's mass ( $M_{hook}$ ) has been set equal to 4.5 kg. At this step, the dimensions of the rest components are not known and consequently we have to assume a value for the total mass of the hoist system ( $M_{hoist}$ ). In our case, this quantity has been considered equal to 170 kg. The correctness of this choice will be checked at a next step of the process.



Fig. 1. View of a typical gantry crane.

TABLE I  
SPECIFICATIONS OF HOIST SYSTEMS WITH WIRE ROPE  
(STANDARDS DIN 15401 AND DIN 15402)

Load mass (tons)	No. of parallel branches	System's efficiency ( $\eta_{hoist}$ )
$\leq 25$	4	0.94
$\leq 75$	8	0.90
$\leq 100$	10	0.87
$> 100$	12	0.85

**Step 3:** “Calculation of the wire and drum diameters”. The diameter ( $d_w$ ) of each wire is specified by (1), where  $M_{load}$  is the load's mass,  $M$  is the force that will be applied at each branch (in kp) given by using (2) and  $k$  is a constant in  $\text{mm/kp}^{1/2}$ . This constant usually takes values between 0.30 and 0.32. The diameter has been found equal to 12 mm and thus the wire rope “B12x160 DIN 655” with a metallic cross-section area ( $A_w$ ) of  $52.7 \text{ mm}^2$  has been selected according to the data found in commercial catalogues. Then, the tensile stress ( $\sigma_z$ ) can be obtained from (3) in  $\text{kp/mm}^2$ . Regarding the drum's diameter ( $d_{drum}$ ), it was found to be equal to 252 mm by using (4), where  $C_1$  is a constant in  $\text{mm/kp}^{1/2}$ , whose value has been set equal to 7 taking into account the specifications of the adopted hoist system. Finally, the bending ( $\sigma_b$ ) and the total stress ( $\sigma_t$ ) are estimated by applying (5) and (6) respectively, where  $E$  is the elasticity module of the wire's material ( $20,000 \text{ kp/mm}^2$  in our case) and  $d$  is the diameter of the rope axis bent over the sheave. If the value of  $\sigma_t$  is much lower than the maximum stress that the wire can withstand, the procedure continues, otherwise its features have to be modified.

$$d_w = k\sqrt{M} \quad (1)$$

$$M = (M_{load} + M_{hoist}) / N \quad (2)$$

$$\sigma_z = M / A_w \quad (3)$$

$$d_{drum} = C_1\sqrt{M} \quad (4)$$

$$\sigma_b = E \frac{d}{d_{drum}} \quad (5)$$

$$\sigma_t = \sigma_z + \sigma_b \quad (6)$$

**Step 4:** “Determination of the pulleys' geometrical parameters”. As already mentioned the hoist system involves two pulleys (a small and a large one) with different diameter. Their diameters ( $D_{p,1}$ ,  $D_{p,2}$ ) can be calculated through (7), where  $C_i$  ( $i=1, 2$ ) is a constant in  $\text{kp/mm}^2$  that has been set equal to 8 and 5 for the large and the small pulley respectively. Then, the geometrical parameter  $B$  (depicted in Fig. 2) is obtained in mm from (8). Considering each pulley

as a cylinder their mass is estimated by using (9), where  $\rho_{steel}$  is the density of the steel used for their construction. Finally, the total mass of the hoist system ( $M_{hoist}$ ) derives by applying (10). The value of this quantity is compared to the corresponding one that was assumed in Step 2. If their ratio (dividing the assumed value with the calculated one) is equal or higher than 2.5, no modification is needed regarding the so far estimated parameters and the process continues. Otherwise, the hoist system has to be re-designed aiming to guarantee its robust construction.

$$D_{p,i} = C_i \sqrt{M} \quad (7)$$

$$B = 4d_w + 20 \quad (8)$$

$$M_{pulley,i} = 0.25\pi D^2 B \rho_{steel} \quad (9)$$

$$M_{hoist} = M_{hook} + M_{pulley,1} + M_{pulley,2} \quad (10)$$

**Step 5: “Determination of the motor’s specifications”.**

The motor’s output power can be calculated by using (11), where  $\eta_{motor}$  and  $\eta_{hoist}$  are the efficiency of the motor and the hoist system respectively and  $g$  is the gravity constant. In the case under study here, we assume that motor will present efficiency at least equal to 0.90, while the efficiency of the hoist system is equal to 0.94 taking into account the data provided in Table I. The total load mass has to be increased by 125%, as defined in the directive “2014/33/EU” of the European Parliament regarding the safety characteristics of the lifting mechanisms. As the LSPMSMs are usually mains-fed machines, their synchronous speed ( $n_m$ ) in rpm is selected taking into account the frequency of the supply system and the poles number. Then, the nominal torque ( $T_{out}$ ) in Nm of the motor derives from (12). The torque required by the load is given using (13), where the total mass is divided by 2, as two pulleys are used. In order to match the torque load with the motor’s torque, the use of a gearbox is necessary. If the derived ratio cannot be implemented by incorporating two tooth gears, a worm gear should be used.

$$P_{out} = \frac{1.25(M_{load} + M_{hoist})g\upsilon}{\eta_{motor} + \eta_{hoist}} \quad (11)$$

$$T_{out} = 9.55P_{out} / n_m \quad (12)$$

$$T_{load} = \frac{(M_{load} + M_{hoist})}{2} g \frac{d_{drum}}{2} \quad (13)$$

The previously described procedure is depicted in flowchart form in Fig. 3. The application of the specific process in our case resulted to a LSPMSM which has to present an output power equal to 7.5 kW and a torque of 71.6 Nm at the speed of 1,000 rpm. To handle the torque requirement, the overall transmission ratio has been set equal to 74:1. Moreover, the ratio of starting ( $T_s$ ) to nominal torque (i.e.  $T_s/T_{out}$ ) is expected to be at least equal to 4 aiming to enhance the system’s lifting capability. Furthermore, the motor’s efficiency ( $\eta$ ) and its power factor ( $\cos\theta$ ) have to be equal or higher than 0.90 and 0.95 respectively.

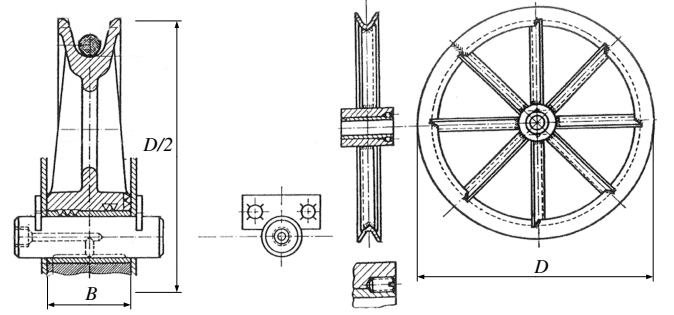


Fig. 2. Detailed representation of the pulley (cross section and side view).

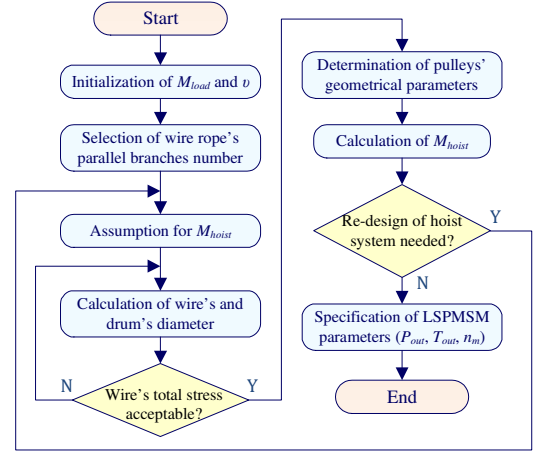


Fig. 3. Proposed procedure for the estimation of motor’s nominal parameters.

#### IV. PROPOSED LSPMSM DESIGN APPROACH

##### A. Preliminary Design

Having set the specifications of the LSPMSM, the classical design methodology has been adopted for the determination of the motor’s basic dimensions, such as its axial length ( $L$ ) and the stator’s inner diameter ( $D_s$ ). For this purpose, the output equation has been used. Also, the international frame sizes and the constraints imposed by them on the aforementioned parameters have been taken into account. Since it was not clear enough how to select the proper value for the ratio  $D_s/L$  and as the number of stator slots ( $Q_s$ ) had not been yet selected, the conduction of a sensitivity analysis was necessary. In this analysis, the value of  $D_s/L$  ratio varied from 0.47 to 0.72 and  $Q_s$  has been considered equal to 18, 36, 54 and 72. A distributed and single-layer winding configuration has been used. For each one of the examined cases, the rest basic dimensions and the slots geometrical parameters were calculated. A detailed view of them is depicted in Fig. 4(a). Since the emphasis here is given on the rotor design, the reader can refer to [19] in order to find more information about the followed design procedure.

TABLE II  
MOTOR VOLUME AS A FUNCTION OF  $Q_s$

No. of slots ( $Q_s$ )	Min. volume (cm <sup>3</sup> )	Max. volume (cm <sup>3</sup> )
18	7273	11278
36	6927	10391
54	7760	10391
72	8357	10472

The minimum and the maximum motor volume that has been obtained for each one of the investigated values of  $Q_s$  is given in Table II. The topologies with 36 slots were finally selected, as they present lower volume and thus a higher torque density.

### B. Rotor Cage Bars Design

The number of the rotor bars ( $Q_r$ ) is also of great importance and it will be examined extensively in this study. In general, it should be chosen so as not to produce too much noise and avoid vibrations, crawling, “cogging” phenomena and cusps in the torque-speed curve. The set of (14) describes general equations for such rotor slots selection strategy [19], where  $p$  is the poles number. Moreover, if  $Q_r$  is divisible by  $p$  the noise during motor’s operation will be minimum. Thus, in our case,  $Q_r$  can be equal to 6, 12, 24 and 48. All these cases have been examined aiming to conclude to the topology that presents the desirable starting performance. Regarding the bars shape, a semi-closed configuration with round cross-section (illustrated in Fig. 4(b)) has been chosen. This type of rotor bar, made of copper, is commonly used in commercial induction motors, which have been designed according to the characteristics of class “D”, where a high starting torque is required as in our case. The reader can find the analytical equations that have been used for the calculation of the rotor slots geometrical parameters in [19].

$$\begin{aligned} Q_s &\neq Q_r \\ Q_s - Q_r &\neq \pm 1, \pm 2, \pm(p \pm 1), \pm(p \pm 2) \\ Q_s - Q_r &\neq \pm p, \pm 3p, \pm 6p, -5p \end{aligned} \quad (14)$$

### C. Permanent Magnets Configuration

Figure 5 shows a schematic view of the investigated topology which has embedded and radially magnetized magnets. Here, the sufficient variables involved are: a) the shaft diameter ( $D_{shaft}$ ), b) the inner diameter ( $D_I$ ), which actually gives the depth from the rotor surface at which the magnets start, c) the closest distance between two adjacent pole magnets ( $R_{ib}$ ), d) the vertical distance from the center of the motor to the middle of the pole magnet ( $O$ ), the magnet’s width ( $w_m$ ) and f) the magnets height ( $h_m$ ).

### D. Proposed Algorithm-based Design Process

The overall proposed rotor design approach is analytically described in flowchart form presented in Fig. 6. Apart from the main script for the overall calculations, an interaction with a FEA software is required for the conduction of 2D transient analysis. The script consists of a main routine and a sub-routine given in Fig. 6(b). The process is organized as follows:

**Step 1:** After the determination of the rotor bars shape the parameter  $D_I$  can be easily calculated, as  $D_I = D_r - 2(h_{r0} + b_{r1} + h_{cr})$ . Next, the values range for parameter  $O$  is specified. Starting with the minimum allowable value for  $O$  the sub-routine for the magnets dimensions calculation is called.

**Step 2:** In this sub-routine, let us donate  $V_j$  ( $j=1..N$ ) the values of the rest three design variables, namely  $w_m$ ,  $h_m$  and  $R_{ib}$  that describe the topology under study. Each variable takes a random value inside its universe of discourse and an appropriate step is defined for it.

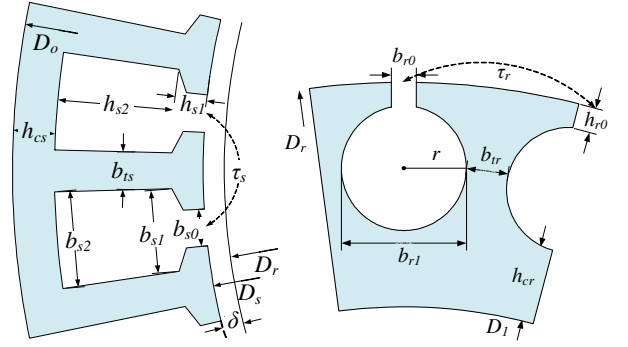


Fig. 4. Geometrical representations of LSPMSM topology: (a) stator slots and (b) rotor bars (without magnets topology and not in scale).

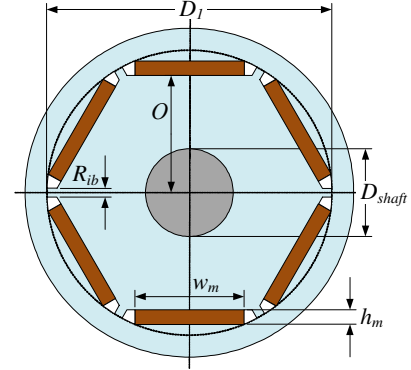


Fig. 5. Detailed view of the rotor's magnets topology under study.

**Step 3:** An iteration loop has been created for each variable. If every variable has been examined, the algorithm stops.

**Step 4:** As the iteration advances, the magnetic field analysis is performed and the starting and steady-state performance are simulated. A few check points follow. Specifically, these check points involve: a) the fulfillment of synchronization in adequate time, b) the achievement of motor’s nominal torque requirements and c) the calculation of  $T_s/T_{out}$  ratio. If the violation of one or more check points is occurred the process returns to Step 2 aiming to re-estimate the values of the three under investigation variables. The algorithm stops when variable index has reached its maximum value. The best solution is stored and the procedure continues with the running of the main routine.

**Step 5:** Then, the efficiency and the power factor of the derived topology are calculated and their values are compared to the corresponding ones that have been set in Section III (i.e.  $\eta \geq 0.90$  and  $\cos\theta \geq 0.95$ ). If the specific requirements are met the process terminates. Otherwise, the permanent magnets position is re-estimated and the sub-routine is called again.

## V. RESULTS AND DISCUSSION

The previously described design procedure was applied to topologies with 36 stator slots, while the rotor bars number has been set consecutively equal to 6, 12, 24 and 48. For each possible configuration 9 different combinations of  $D_s$  and  $L$  were also tested. Consequently, the total number of the examined motor topologies was equal to 36. The post-processing analysis of the derived-results revealed that all the



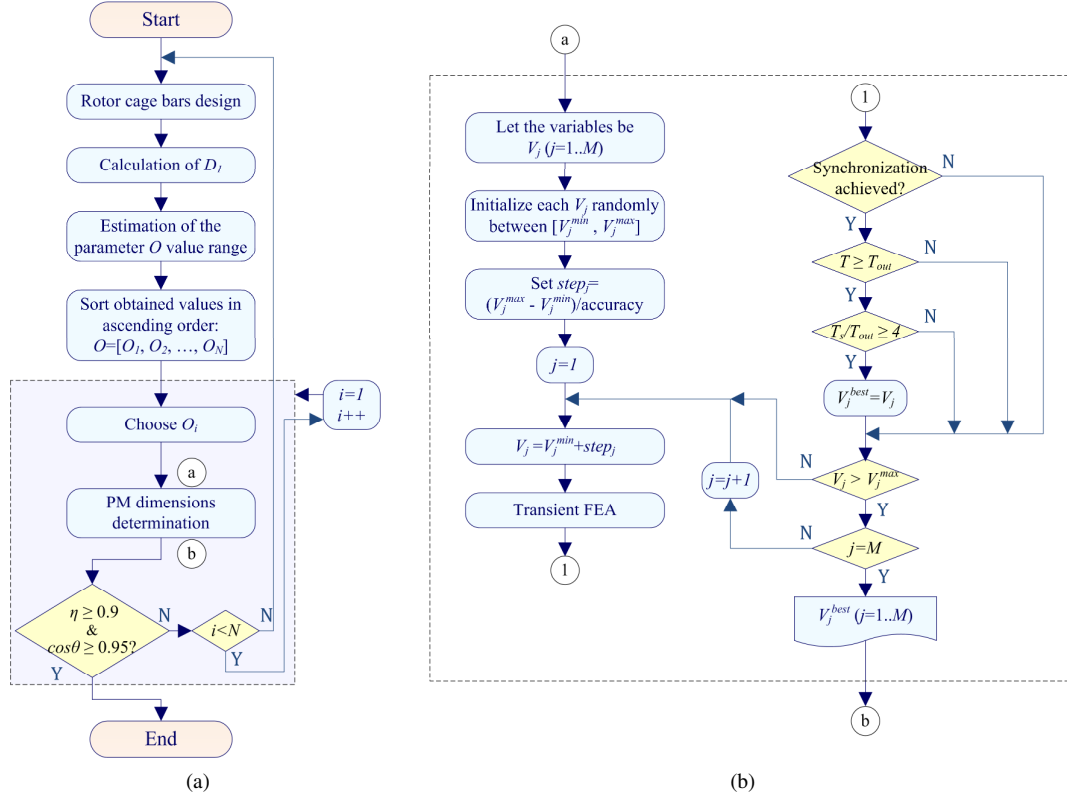


Fig. 6. Flowchart of the proposed LSPMSM design methodology: a) Overall scheme and b) detailed view of the sub-routine used for the calculation of the permanent magnets' position and dimensions.

investigated topologies succeeded to reach the synchronous speed in adequate time ( $\sim 120\text{ms}$ ) and their synchronization capability has been considered as satisfactory. The rotor configurations with 6, 12 and 24 rotor bars failed to meet the set starting torque requirements. In these cases, the maximum value for the ratio  $T_s/T_{out}$  was found equal to 1.62, 1.88 and 3.67 respectively and thus they have been rejected. When 48 rotor bars were used, the specific ratio varied from 4.13 to 5.80. The 9 topologies with 48 rotor bars were further investigated and compared to each other in terms of torque density, stator winding's current density, starting current, etc.

A 2D cut-out view (1/6<sup>th</sup> part) of the proposed LSPMSM topology is illustrated in Fig. 7, where the flux density distribution over its various parts is also given. As it can be seen, no severe saturation has been occurred. The motor's geometrical parameters are summarized in Table III. Its net mass is equal to 48.95 kg, leading to a torque density of 1.46

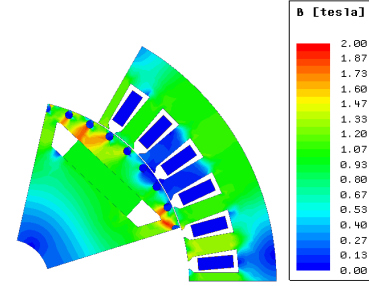


Fig. 7. Flux density distribution of the proposed topology at full-load.

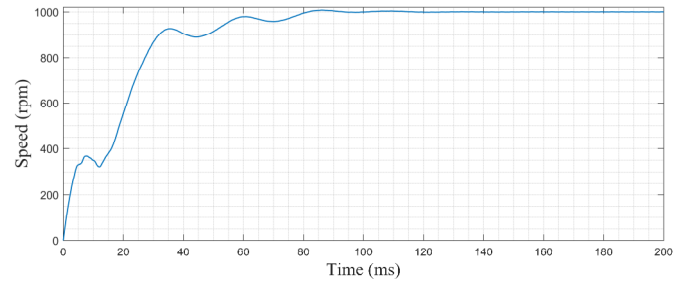


Fig. 8. Speed versus time curve of the proposed topology.

TABLE III  
GEOMETRICAL CHARACTERISTICS OF THE PROPOSED LSPMSM TOPOLOGY

Quantity	Value (mm)	Quantity	Value (mm)
Stator's outer/inner diameter ( $D_o/D_s$ )	210/142	Stator tooth tip height/slot height ( $h_{st}/h_{ss}$ )	2.0/17.4
Motor's axial length ( $L$ )	220	Rotor bar width/height at the opening ( $b_{ro}/h_{ro}$ )	1.5/0.5
Rotor's outer/shaft Diameter ( $D_r/D_{shaft}$ )	141/33	Rotor bar diameter ( $b_{rl}$ )	3
Inner diameter ( $D_i$ )	129	PM width/height ( $w_m/h_m$ )	34/9
Slot opening/base /top width ( $b_{so}/b_{s1}/b_{s2}$ )	3.0/6.1/9.1	Distance $O/R_{ib}$	50/10

Nm/kg, while the magnets mass is equal to 2.9 kg. During the nominal performance, the efficiency and the power factor were calculated to be equal to 90.3% and 0.95 respectively. The above characteristics coincide with the requirements set by the standard "IEC 60034-30-1" regarding the industrial line motors with premium efficiency (IE3). A stator winding's current density of 6 A/mm<sup>2</sup> has been achieved and thus it would be necessary for the motor to be fan-cooled taking into account its heavy-duty cycle. Furthermore, the ratio between the starting current ( $I_s$ ) and the nominal one

( $I_N$ ) is equal to 6.7, which can be considered acceptable, as the motor provides a torque of 313 Nm during the start-up phase. The synchronous speed is achieved at about 120 msec after its starting-up according to the curve depicted in Fig. 8 and no severe oscillations are observed. Finally, the torque ripple at the steady-state performance was found to be less than 8%.

## VI. CONCLUSIONS

A simple but effective multi-criteria design approach is presented in this paper that could ease the design process of LSPMSMs. The applied algorithm based procedure resulted to a lower number of iterations needed and thus minimized the computational cost. The derived topology exhibits enhanced start-up and synchronization capability, while simultaneously fulfils the requirements of premium-efficient industrial motors. The proposed approach has been successfully applied in a motor for gantry crane application.

## VII. REFERENCES

- [1] B. Stumberger, T. Marcic, M. Hadziselimovic, "Direct comparison of induction motor and line-start IPM synchronous motor characteristics for semi-hermetic compressor drives", *IEEE Transactions on Industry Applications*, vol. 48, issue 6, pp. 2310-2321, Nov./Dec. 2012, doi: 10.1109/TIA.2012.2227094.
- [2] M. N. Azari, M. Mirsalim, "Analytic modelling of a line-start permanent-magnet motor with slotted solid rotor", *IET Electric Power Applications*, vol. 8, issue 7, Aug. 2014, pp. 278-285, doi: 10.1049/iet-epa.2014.0018.
- [3] X. Lu, K. L. V. Iyer, K. Mukherjee, N. C. Kar, "Development of a novel magnetic circuit model for design of premium efficiency three-phase line start permanent magnet machines with improved starting performance", *IEEE Transactions on Magnetics*, vol. 49, no. 7, pp. 3965-3968, July 2013, doi: 10.1109/TMAG.2013.2242869.
- [4] A. H. Isfahani, S. Vaez-Zadeh, "Effects of magnetizing inductance on start-up and synchronization of line-start permanent-magnet motors", *IEEE Transactions on Magnetics*, vol. 47, issue 4, pp. 823-829, Apr. 2011, doi: 10.1109/TMAG.2010.2091651.
- [5] A. D. Aliabad, M. Mirsalim, "Analytic modelling and dynamic analysis of pole-changing line-start permanent-magnet motors", *IET Electric Power Applications*, vol. 6, issue 3, Mar. 2012, pp. 149-155, doi: 10.1049/iet-epa.2011.0146.
- [6] D. Stoia, M. Cernat, A. A. Jimoh, D. V. Nicolae, "Analytical design and analysis of line-start permanent magnet synchronous motors", in *Proceedings of 2009 AFRICON Conference*, Nairobi, Kenya, Sept. 23-25, 2009, doi: 10.1109/AFRCON.2009.5308177.
- [7] C. Jedryczka, K. Knypinski, A. Demenko, J. K. Sykulski, "Methodology for cage shape optimization of a permanent magnet synchronous motor under line start conditions", *IEEE Transactions on Magnetics*, vol. 54, issue 3, Mar. 2018, doi:10.1109/TMAG.2017.2764680.
- [8] C. Jedryczka, R. M. Wojciechowski, A. Demenko, "Influence of squirrel cage geometry on the synchronization of the line start permanent magnet synchronous motor", *IET Science, Measurement & Technology*, vol. 9, issue 2, pp. 197-203, Mar. 2015, doi: 10.1049/iet-smt.2014.0198.
- [9] E. P. Sanchez, A. C. Smith, "Line-start permanent-magnet machines using a canned rotor", *IEEE Transactions on Industry Applications*, vol. 45, no. 3, pp. 903-910, May/June 2009, doi: 10.1109/TIA.2009.2018981.
- [10] T. Ding, N. Takorabet, F. M. Sargos, X. Wang, "Design and analysis of different line start PM synchronous motors for oil pump applications", *IEEE Transactions on Magnetics*, vol. 45, no. 3, pp. 1816-1819, Mar. 2009, doi: 10.1109/TMAG.2009.2012772.
- [11] Y. L. Karnavas, I. D. Chasiotis, "A computational efficient algorithm for the design of a line start synchronous motor with multi-segment magnet rotor", in *Proceedings of IEEE Workshop on Electrical Machines Design, Control and Diagnosis (WEMDCD)*, Torino, Italy, Mar. 26-27, 2015, Cd. Ref. no: 302.
- [12] R. T. Ugale, B. N. Chaudhari, S. Baka, A. Pramanik, "A hybrid interior rotor high-performance line start permanent magnet synchronous motor", *Electric Power Components and Systems*, vol. 42, issue 9, pp. 901-913, 2014, doi: 10.1080/15325008.2014.903539.
- [13] J. X. Shen, Peng Li, M. J. Jin, G. Yang "Investigation and countermeasures for demagnetization in line start permanent magnet synchronous motors", *IEEE Transactions on Magnetics*, vol. 49, no. 7, pp. 4068-4071, July 2013, doi: 10.1109/TMAG.2013.2244582.
- [14] A. D. Aliabad, M. Mirsalim, N. F. Ershad, "Line-start permanent-magnet motors: significant improvements in starting torque, synchronization and steady-state performance", *IEEE Transactions on Magnetics*, vol. 46, no. 12, pp. 4066-4072, Dec. 2010, doi: 10.1109/TMAG.2010.2070876.
- [15] S. F. Rabbi, M. L. Little, M. A. Rahman, "A novel technique using multiresolution wavelet packet decomposition for real time diagnosis of hunting in line start IPM motor drives", *IEEE Transactions on Industry Applications*, vol. 43, issue 3, pp. 3005-3019, May/June 2017, doi: 10.1109/TIA.2016.2633541.
- [16] M. N. Azari, M. Mirsalim, S. M. A. Pahnehkolaei, S. Mohammadi, "Optimum design of a line-start permanent-magnet motor with slotted solid rotor using neural network and imperialist competitive algorithm", *IET Electric Power Applications*, vol. 11, issue 1, 2017, doi: 10.1049/iet-epa.2016.0109.
- [17] Bo Yan, X. Wang, Y. Yang, "Comparative parameters investigation of composite solid rotor applied to line-start permanent-magnet synchronous motor", *IEEE Transactions on Magnetics*, vol. 54, no. 11, Nov. 2018, doi: 10.1109/TMAG.2018.2844550.
- [18] S. F. Rabbi, M. L. Little, M. A. Rahman, "A novel technique for detection and analysis of hunting in line-start IPM motors using stator current signature", in *Proceedings of 2016 IEEE Industry Applications Society Annual Meeting*, Portland, OR, USA, Oct. 2-6, 2016, doi: 10.1109/IAS.2016.7731840.
- [19] T. A. Lipo, "Introduction to AC machine design", Wiley-IEEE Press, Oct. 2017, ISBN: 978-1-119-35216-7, 544 pages.

## VIII. BIOGRAPHIES

**Ioannis D. Chasiotis** was born in Athens, Hellas, 1991. He received the Diploma Degree from the Dept. of Electrical and Computer Engineering (DECE), Democritus University of Thrace (DUTH), Xanthi, Hellas, in 2015. He is with the Electrical Machines Laboratory of the same Department where he is currently pursuing his PhD degree. He has gained a full time award scholarship from Onassis Foundation for his post-graduate studies.

His research interests are in the area of electrical machines design, the incorporation of artificial intelligence methods in the design process and the development of permanent magnet synchronous and induction machines with characteristics of high power density and high efficiency.

Mr. Chasiotis is a Chartered electrical engineer and member of Hellenic Technical Chamber and Student Member of IEEE.

**Yannis L. Karnavas** was born in Volos, Hellas, 1969. He received the Diploma Degree and his PhD from the Dept. of Electrical and Computer Engineering (DECE), Democritus University of Thrace (DUTH), Xanthi, Hellas, in 1994 and 2002 respectively.

From 2004 to 2013 was Director of the Electrical Machines & Electrical Installations Laboratories of Dept. of Electrical Engineering (TEI of Crete, Hellas). Since 2013 he is with the Electrical Machines Laboratory of the DECE, DUTH. His research interests include electrical machines design, analysis, modeling and optimization as well as AI methods application to the above areas. He has published several papers in various international journals and conferences as well as book chapters in international engineering books. He has participated in research projects as research leader or scientific associate. He serves as an Associate Editor and as an Editorial board member in various international scientific journals.

Prof. Karnavas is a Chartered electrical engineer as well as a member of Hellenic Technical Chamber. He is also a member of IEEE, Power Engineering Society (PES), Industry Applications Society (IAS) and Industrial Electronics Society (IES).

**Stylianios I. Dimadis** was born in Agrinio, Hellas, 1994. He received the Diploma Degree in Electrical and Computer Engineering from the Dept. of Electrical and Computer Engineering, Democritus University of Thrace, Xanthi, Hellas, in 2018. He is with the Electrical Machines Laboratory of the same Department. His research interests are in the area of electrical machines design for industrial applications.